PHYSICAL REVIEW C **69**, 031302(R) (2004)

Low-lying levels in ^{15}F and the shell model potential for drip-line nuclei

V. Z. Goldberg,* G. G. Chubarian, G. Tabacaru, L. Trache, and R. E. Tribble
Texas A&M University, Cyclotron Institute, College Station, Texas 77843-3366, USA

A. Aprahamian, G. V. Rogachev, and B. B. Skorodumov
University of Notre Dame, Notre Dame, Indiana 46556, USA

X. D. Tang
Argonne National Laboratory, Argonne, Indiana 60439, USA
(Received 12 December 2003; published 17 March 2004)

The ground and first excited states in ^{15}F were studied in resonant elastic scattering using the thick (CH_4) gas target method in inverse kinematics with a separated ^{14}O beam. An analysis of the excitation functions of the elastic scattering was carried out with the potential model. The quantum numbers $1/2^+$ (ground state) and $5/2^+$ (first excited state) were assigned to the lowest two states in ^{15}F. Also, the widths and the proton decay energies of the unbound levels were obtained. The analysis of the data indicates that a large diffuseness is needed in the Woods-Saxon potential in order to describe single-particle features in drip-line nuclei.

DOI: 10.1103/PhysRevC.69.031302 PACS number(s): 27.20.+n, 25.40.Cm, 25.60.Bx, 21.10.Dr

Over the past decade it has become clear that drip-line nuclei demonstrate a number of phenomena which are not found in nuclei close to the line of stability. One such feature is the change in magic numbers, which are generated by a conventional Woods-Saxon potential with parameters fitted for stable nuclei [1–3]. One example is the intruder single-particle $2s_{1/2}$ state, which appears to be the ground state in ^{11}Be [4] and ^{11}N [5] instead of the $1p_{1/2}$ state. As another example, it has been predicted [1–3] that the diffuseness of nuclear densities for intermediate mass nuclei increases dramatically when approaching the neutron drip line. These phenomena indicate that the parameters of the shell model potential can be unusual for nuclei at the borders of nuclear stability. Figure 1 shows how, for a light nucleus, the energies of the shell model levels in a Woods-Saxon potential depend on the ratio of the diffuseness to radius parameters. It can be seen in Fig. 1 that the $1p_{1/2}$ and $2s_{1/2}$ levels approach each other as the ratio increases. One way to explain the phenomena observed near the drip line is that the single-particle potential changes its shape giving way to new shell structure. This effect can be tested by an analysis of the nucleon widths of the single-particle states in drip-line nuclei, which are mainly dependent upon the geometrical parameters of the well.

^{15}F is a good system to check the considerations above. The lowest states in ^{15}F are unstable to proton decay and should have dominantly single-particle structure. The theoretical predictions for the single-particle spectroscopic factors are 0.94 [4] and 0.97 [6]. The first experiments on ^{15}F observed the ground state and the first excited state [7,8]. The spins and parities $1/2^+$ and $5/2^+$ were assigned using information from the analog nucleus, ^{15}C. The ^{15}F states were populated in the multinucleon transfer reaction ^{20}Ne(^{3}He, ^{8}Li)^{15}F, which had very low cross section. As a result, the data on the level positions and their widths differ by more than 100 keV from the two measurements. Recently ^{14}O+p scattering was reported [9] based on results of resonance scattering of ^{14}O on hydrogen with the thick target inverse kinematics method [5,10,11]. An approach similar to Ref. [9] was used in the present experiment. However, there are important differences in the details of the two measurements. In the present work, a gas target, CH_4, was used instead of a solid CH_2 target. The gas target results in a drastic decrease of the background (see below). Also, only the excitation function at 180° (c.m.) in arbitrary units was measured in Ref. [9], while in the experiment reported here measurements were made at several angles. As a result, we have a better determination of the positions and the widths of the levels which allows us to make conclusions about the parameters of the interaction potential between ^{14}O and protons.

The experiment was performed at the Texas A&M University Cyclotron Institute. A ^{14}N beam was accelerated by

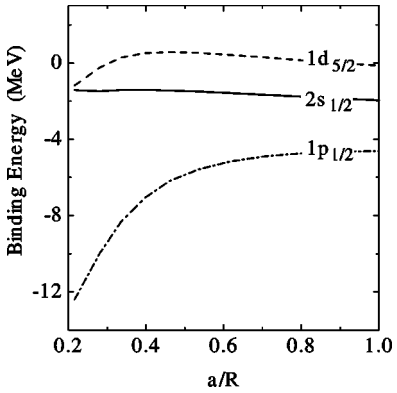

FIG. 1. Shell model neutron binding energies vs the ratio of the diffuseness parameter to the radius of the potential. The calculations are made for a light nucleus ($A=11$), starting with typical parameters $V_0=-55$ MeV, $V_{ls}=6$ MeV, $R=r_0A^{1/3}$, $r_0=r_0(ls)=1.2$ fm, $a=a_{ls}=0.6$ fm, and keeping $a+R=$const.

*Electronic address: goldberg@comp.tamu.edu

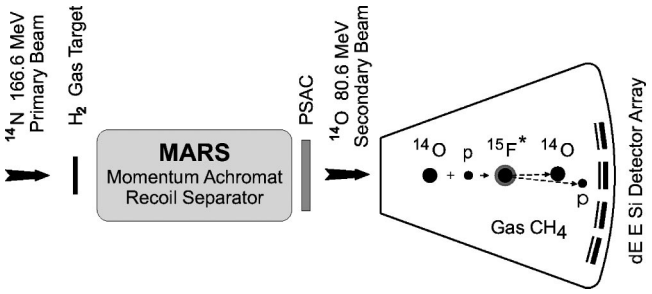

FIG. 2. Experimental setup.

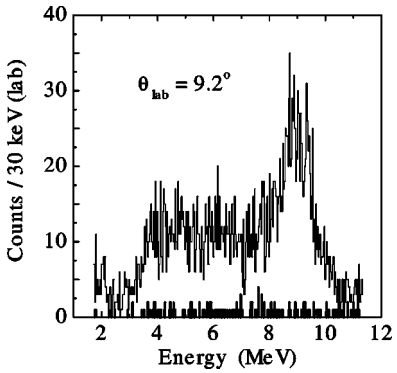

FIG. 3. Experimental excitation function. The background is shown with thick bars at the bottom of the figure.

the K500 superconducting cyclotron to 11.9 MeV/nucleon. The beam bombarded a hydrogen gas target of 9 cm length at LN_2 temperature and 1.9 atm pressure with 4μm Havar entrance and exit windows. The recoil spectrometer MARS [12] was used to filter reaction products to produce the ^{14}O secondary beam. A beam purity of 99.9% was obtained with the admixtures being ^{7}Be and protons. The excitation function of $^{14}O+p$ elastic scattering was measured in a chamber filled by methane gas that was placed at the MARS focal plane (Fig. 2). A position sensitive avalanche counter (PSAC) was positioned before the entrance to the scattering chamber to obtain position and timing information for each particle of the secondary beam. The efficiency of the PSAC was 100% at the available intensity of the ^{14}O beam of 10^4pps, so it also determined the total number of ^{14}O events. The angular divergence of the beam was 1.2°.

The radioactive beam entered the scattering chamber through a 12 μm thick organic foil. The ^{14}O beam energy after the foil was 80.6 MeV with an energy spread of 1.5%. The 50 cm long chamber was filled with methane gas of 99.0% purity at a pressure 310 Torr. The pressure of the gas was adjusted so that the beam stopped before the detector placed at 0°. Due to the large difference in energy loss, the recoiling protons, created by the elastic scattering of ^{14}O on hydrogen, easily penetrated through the gas into the array of ΔE-E Si detectors. Four detector telescopes were positioned at 0°, −7.5°, +9.2°, and +16.5° relative to the beam direction at the entrance window. Two ΔE detectors had thicknesses of 75 μm, and two were 1 mm thick. This allowed for a more precise energy calibration of the broad part of excitation function without summing two detectors in the telescope. More details of the method can be found elsewhere [5,10,11]. Particle identification of the recoil protons was made by $\Delta E-E$ and time of flight (TOF) analysis; time of flight being given by signals from the PSAC and ΔE detectors. Using the TOF-ΔE analysis, it was possible to identify the low energy protons, which stopped in the ΔE detectors.

In addition to the CH_4 gas, data were obtained with CO_2 gas, to subtract background events from interactions with the carbon in the methane gas. Figure 3 shows the experimental excitation function for the 9.2° angle together with the results of the background run. The background rate, as seen in Fig. 3, is very small. It is much smaller then in the experiment of Ref. [9], especially at low proton energy. Consequently, background subtraction does not influence the precision of the final results. The difference in the background level in the present work and in Ref. [9] can be only partly attributed to the higher abundance of hydrogen in CH_4. The other factors are the different initial energies of ^{14}O and the difference in solid angle for the elastic scattering and background events. The proton spectra produced by the interaction of ^{14}O with ^{12}C are nearly continuous, with a maximum at low energies, a bit above the Coulomb barrier. These protons originated mainly from the highest energy ^{14}O ions prior to when they lost part of their energy in the target. In the case of a solid target, the solid angle for different energies of ^{14}O is the same (the solid target is very thin compared to the distance to a detector). In the present experiment the solid angle is small for interactions near the front of the target and large for interactions near the back of it. Consequently, the low energy protons produced by the interaction of low energy ^{14}O with hydrogen, are detected with much higher solid angle than the background protons from interaction of high energy ^{14}O with ^{12}C. The detectors were calibrated using an α source at the beginning of the experiment, between experimental runs, and at the end. During measurements, the detector at 0° deteriorated, and its data were excluded from the detailed analysis.

The excitation functions for the elastic $^{14}O+p$ scattering in the c.m. system are shown in Fig. 4. As can be seen in Fig. 4, different regions of the excitation functions which were measured at the same angle in the laboratory system, correspond to different angles in the c.m. system due to the long path of the beam in the gas. The structure of the curves in Fig. 4 is due to Rutherford scattering at low energies, a dip at 1.1 MeV due to the interference between Rutherford scattering and a broad resonance at 1.5 MeV, and a peak of a few hundred keV width at 2.8 MeV. The experimental resolution in the region of 2.8 MeV peak was about 25 keV (the main contributions are the size of the beam spot; beam angular and energy spread, 18 keV; and straggling in the gas, 14 keV) and deteriorated at lower energies, reaching 75 keV near 1 MeV. Convoluting the experimental resolution function with the predicted yield curve did not produce any noticeable effect in the χ^2 analysis. The absolute calibration of energies in the c.m. system is better than ±15 keV, which is dominated by the uncertainty in the angle of the incoming beam and the uncertainty in the energy loss of ^{14}O in methane, which was taken to be 7%. The absolute cross sections were obtained with a precision of ±7%.

The experimental excitation functions were fit by means

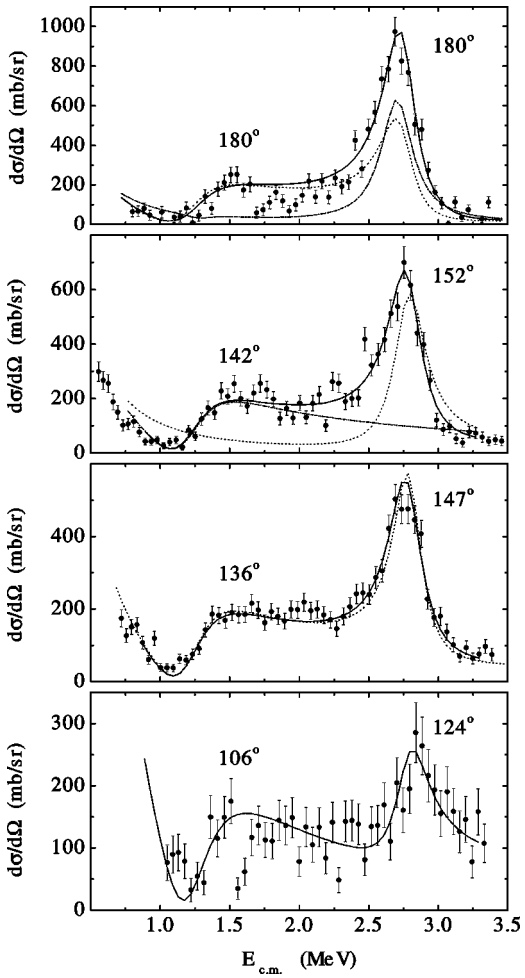

FIG. 4. Excitation functions for the $^{14}O+p$ elastic scattering. The solid lines are fits with the parameters shown in the fourth column of Table I. The angles indicated in the pictures are the c.m. angles for two energies, 2.8 and 1.5 MeV. The top panel shows the 0° excitation function. The dotted curve shows the fit assuming a $1/2^+$ ground state and $3/2^+$ excited state. The dash-dotted curve shows the fit assuming a $1/2^-$ ground state and $5/2^+$ excited state. The second panel shows the separate contributions of *s* wave (dot-dashed line) and *d* wave (dotted line). The dashed line in the third panel shows the best fit which has a diffuseness parameter of 0.64 fm.

of a Woods-Saxon potential with a spin-orbit term but no imaginary part. The initial parameters of the potential were fixed by fitting the lowest $5/2^+$ and $1/2^+$ levels in ^{17}O(^{17}F) using a "reasonable" set of parameters [13,14], which are given in Table I. The Woods-Saxon potential with this set of parameters generates correct energies for the ground and the first excited states in ^{17}O and ^{17}F to within about 100 keV. (In this approach we neglect corrections, such as *p*-*n* mass and magnetic moment difference. The effect of these correction could indeed be about 100 keV [15]). The potential also generates the $d_{3/2}$ state in ^{17}O at 5.35 MeV excitation energy which is between two known $3/2^+$ levels at 5.1 and 5.9 MeV, but closer to the level (5.1 MeV) with the larger spectroscopic factor [14]. After modifying the V_0 parameter to account for the removal of two protons from ^{16}O [13], a

TABLE I. Parameters of the Woods-Saxon potential.

Parameters	^{17}O/^{17}F	^{15}C	^{15}F
V_0	−58.9	−54.15	−53.67[a]
V_{sl}	6.4	6.4	6.4
r_0	1.17	1.17	1.17
$r_0(sl)$	1.17	1.17	1.17
r_0(Coulomb)	1.21	1.21	1.21
a	0.64	0.71	0.735
a_{sl}	0.64	0.64	0.64
	Nucleon binding energy (MeV)		
$1/2^+$	3.270/0.105	1.218	−1.290
$5/2^+$	4.140/0.600	0.478	−2.795

[a]For the *s* state $V_0=-53.27$.

calculation was carried out to obtain the energies of the two lowest states in ^{15}C. This results in too much binding for the states in question, but, what is more important, the calculated levels are nearly degenerate.

There are two options to increase the spaces between the $2s_{1/2}$ and $1d_{5/2}$ states in the Woods-Saxon based calculation: (1) increase the diffuseness parameter; (2) decrease the strength of the spin-orbit potential. In the second option, the energy splitting between the $1d_{5/2}$ and $1d_{3/2}$ levels decreases resulting in the $1d_{3/2}$ excitation energy in ^{15}C being below 4.7 MeV. But no $3/2^+$ level in ^{15}C has been identified around this energy [16]. The closest level to this region with an unknown spin is at 5.8 MeV. Therefore, we chose to change the diffuseness parameter. The parameters which generate the experimental values of the excitation energies of the first two states in ^{15}C are shown in the third column of Table I.

These potential parameters were used to fit the measured excitation functions. The changes in c.m. angle with excitation energy for each detector were taken into account. The parameter V_0, which influences the level positions, and a, which influences the width and the position of the levels, were varied to define a two dimensional χ^2 area. Then a simple function, $u(a,V_0)$, of the level position was determined and the single parameter dependence of χ^2 was defined. The data obtained with the 0° and the largest angle detectors were excluded from the fit. The latter was excluded due to low counting statistics. Good agreement is obtained with all experimental excitation functions using the same set of potential parameters, as can be seen in Fig. 4. The new resonance parameters from the fit are summarized in the fourth and the fifth column of Table II. The uncertainties correspond to one standard deviation of the values.

Other possible spin assignments were considered for the states in question but the calculations clearly showed that the character of the broad structures in Fig. 4 and the interference with the Coulomb scattering determines unique spin assignments. The fit at different angles verifies the assignments made. As an illustration, a fit with a $1/2^-$ resonance (instead of $1/2^+$) and a fit with $3/2^+$ (instead of $5/2^+$) are shown in the figure.

TABLE II. Parameters of low-lying resonances in ^{15}F.

Level	Ref.	I^{π}	Decay energy (MeV)	Width (MeV)
	[7]	$(1/2^+)$	1.6 ± 0.2	$\geqslant 0.9$
	[8]	$(1/2^+)$	1.37 ± 0.18	0.8 ± 0.3
g.s.	[17]	$(1/2^+)$	1.41 ± 0.15	0.8 ± 0.3
	[9]	$1/2^+$	1.51 ± 0.15	1.2
	This work (Ψ)	$1/2^+$	$1.29^{0.08}_{0.06}$	0.7
	This work ($\delta^{90°}$)	$1/2^+$	$1.45^{0.16}_{0.1}$	
	[7]	$(5/2^+)$	2.8 ± 0.2	0.24 ± 0.03
	[8]	$(5/2^+)$	2.67 ± 0.1	0.5 ± 0.2
First exc.	[17]	$(5/2^+)$	2.54 ± 0.07	0.27 ± 0.07
	[9]	$5/2^+$	2.853 ± 0.045	0.34
	This work	$5/2^+$	2.795 ± 0.045	0.325 ± 0.06

Information about the low-lying states in ^{15}F is given in Table II. The most precise results come from resonance scattering. Even with small beam intensities, significant improvements in counting statistics have been obtained in the resonance scattering measurements compared to the results obtained through multinucleon transfer reactions with stable beams. Generally the data in Table II are in reasonable agreement with the exception of the result from Ref. [17] for the excitation energy of the first excited state. A more detailed comparison of the resonance scattering results of Ref. [9] and the present work indicates a systematic difference of about 60 keV in the energies of both levels. It might be due to the difficulties of taking into account the large angular spread of the ^{14}O beam in Ref. [9]. As can be seen in Table II, the energies of the states given by Ref. [9] are higher than the other results shown in the table.

The width of the excited state was obtained through the resonance fit. The uncertainty in the width determination is mainly due to the fact that it is large. Also, interference with the very broad ground state adds to the uncertainty. The value for the width found in the present analysis, 325 keV, is in a good agreement with the result of 340 keV found in Ref. [9], but no uncertainty was quoted there. Also the present value is in good agreement with the other results presented in the table.

The ground state of ^{15}F is a broad resonance. Thus it is necessary to specify what is meant by its energy and width. In the potential approach one can find the maximum of the resonance wave function versus energy, and the maximum of the cross section of the elastic scattering, which corresponds to the 90° phase shift. These values are the same for a narrow resonance. For the case of the broad $1/2^+$ resonance, the difference is about 150 keV. (Similar results for the broad $1/2^+$ levels were also obtained earlier, see Refs. [5,9]). The same problem occurs when extracting the width. If the separated contribution of the $1/2^+$ resonance is considered, the width (full width at half maximum) of the resonance is about 1.2 MeV. But the peak is highly asymmetric due to the change in sign of the interference with the Coulomb interaction. The phase shift of the Coulomb interaction subtracts from the resonance phase at lower energies and adds to it at higher energies. Also, the nuclear potential phase increases with energy. Therefore the features of the resonance are highly distorted by the interplay of the interference with the potential scattering. It is quite possible that the resonance in question would manifest a different width in a direct reaction because of the off shell amplitude contributing to the transfer of a nucleon. The calculation, which is based on the behavior of the wave function in the potential well, results in a 700 keV resonance width, which is closer to that observed in the direct reactions.

In Table II we present two results for the energy of the resonance, one corresponding to the maximum of the cross section (90°) and the other corresponding to the maximum of the wave function. The calculations, based on the fall-off of the maximum of the wave function, were used to obtain the width in Table II. The parameters, which were obtained by the fit to the binding energy of a neutron in two lowest states in ^{15}C, and the ones obtained by the fit to the energies and widths of the mirror levels in ^{15}F are practically the same. The uncertainty of the width is correlated to the precision with which the diffuseness parameter, a, is determined, $0.65 \leqslant a \leqslant 0.82$. Hence a larger diffuseness parameter than for the ^{17}O(^{17}F) case is needed to describe the level positions in ^{15}C and ^{15}F, as well as the widths of the particle unstable states in ^{15}F.

The only other way to describe the large experimental widths of the single-particle states in question is to increase the radius parameter, r_0. In order to describe the width, r_0 must be increased up to over 1.3 fm, which makes the radius parameter of ^{15}F greater than that of ^{17}F and destroys the fit to $2s_{1/2}$ and $1d_{5/2}$ levels with the same well depth parameter. We note that in Ref. [9], the authors needed a potential with a large diffuseness parameter, $a=0.75$ fm, to fit the data in spite of a larger r_0 parameter of 1.25 fm.

The results obtained for the geometry of the potential for ^{15}F assumed that the single-particle spectroscopic factor (or the reduced width) is very close to the single-particle limit, in agreement with theoretical predictions. If the spectroscopic factor is less than the single-particle limit, it would mean that the single-particle width is larger than the value that was found. This, in turn, would mean that the geometry

parameters would need even a larger change than has been demonstrated here.

The ground and first excited states in ^{15}F were measured using the thick target method in inverse kinematics. The analysis of the data was made in the framework of the potential model. The analysis results in unique spin-parity assignments for the states of $1/2^+$ and $5/2^+$, respectively. ^{15}F is unbound with respect to one-proton decay by 1.29 or 1.45 MeV depending on the model interpretation of the position of this broad resonance ($\sim$700 keV). The first excited state is unbound with respect to one-proton decay by 2.795 ± 0.045 MeV and its width is 325 ± 60 keV. The data on the energies of the lowest levels in ^{15}C and ^{15}F together with the width of the excited state in ^{15}F give strong evidence for a large diffuseness of the nuclear potential that is needed to describe single-particle features in drip-line nuclei.

The authors appreciate stimulating discussions with Professor A. Mukhamedzhanov and Professor E. Saperstein. This work was supported by the Department of Energy Grant No. DE-FG03-93ER40773 and the National Science Foundation Grant No. PHY02-030099.

[1] J. Dobaczewski *et al.*, Phys. Rev. Lett. **72**, 981 (1994).
[2] R. F. Casten and B. M. Sherrill, Prog. Part. Nucl. Phys. **45**, S171 (2000).
[3] E. E. Saperstein and S. V. Tolokonnikov, JETP Lett. **78**, 343 (2003).
[4] F. Ajzenberg-Selove, Nucl. Phys. **A433**, 1 (1985).
[5] L. Axellsson *et al.*, Phys. Rev. C **54**, R1511 (1996).
[6] A. Brown (private communication).
[7] W. Benenson *et al.*, Phys. Rev. C **17**, 1939 (1978).
[8] G. J. KeKelis *et al.*, Phys. Rev. C **17**, 1929 (1978).
[9] W. Peters *et al.*, Phys. Rev. C **68**, 034607 (2003).
[10] V. Z. Goldberg, Clustering Phenomena in Atoms and Nuclei, Springer Series in Nuclear and Particle Physics.
[11] G. Rogachev, Ph.D. thesis, Kurchatov Institute, Moscow, 1999.
[12] R. E. Tribble *et al.*, Nucl. Phys. **A701**, 278 (2002).
[13] A. Bohr and B. R. Mottelson, *Nuclear Structure* (Benjamin, New York, 1969), Vol. 1.
[14] F. Ajzenberg-Selove, Nucl. Phys. **A305**, 1 (1982).
[15] J. A. Nolen and J. P. Schiffer, Annu. Rev. Nucl. Sci. **19**, 471 (1969).
[16] F. Ajzenberg-Selove, Nucl. Phys. **A449**, 1 (1986).
[17] A. Lepine-Szily *et al.*, Nucl. Phys. **A722**, 512c (2003).